Enhancement of polarization anisotropy in ultrafast carrier dynamics by intramolecular excitation in the organic conductor κ-(BEDT-TTF)$_2$Cu(NCS)$_2$

K. Nakagawa[1], T. Sato[1], S. Tsuchiya[1] [(a)], J. Yamada[2] and Y. Toda[1]

[1] *Department of Applied Physics, Hokkaido University, Hokkaido 060-8628, Japan*
[2] *Graduate School of Material Science, University of Hyogo, Hyogo 678-1205, Japan*

PACS 78.47.+p – First pacs description
PACS 74.70.Kn – Second pacs description

Abstract –In this work, in order to investigate the origin of the anomalous polarization dynamics observed in the normal conducting state of the organic superconductor κ-(BEDT-TTF)$_2$Cu(NCS)$_2$, we performed optical pump-probe measurements by varying the probe pulse energy from $\hbar\omega_{pr} = 1.44$ to 1.59 eV. We found that the polarization-dependent transient signal was most enhanced at ~ 1.51 eV, which was close to the intramolecular excitation energy ~ 1.41 eV of the BEDT-TTF molecules but is not exactly matched. This difference is linked to the formation of an energy gap at the Fermi energy at low temperatures, which results in an increase or decrease in pump-induced absorption between the states near the Fermi energy and the intramolecular excited states depending on probe polarization. In other words, the intramolecular excitation at 1.41 eV, which has a strong polarization dependence, serves as a probe of the dynamics involved in gap formation. A simple calculation shows that the size of the gap is ~ 0.20 eV, which is close to that of the BEDT-TTF based Mott insulators. It is suggested that the gap arises from the phase-separated Mott state caused by photoinduced modulation of effective electron correlation.

Introduction. – Recently, metastable states that can be reached by photoexcitation have been actively explored in strongly correlated electronic materials for fundamental research of non-equilibrium phase transitions and device applications [1]. In a perovskite manganite crystal [2] and organic molecular salt, [3] the photoexcitation causes the charge-order melting, leading to the transient metallic state. Alternatively, an electronic ordered state, such as superconductivity, which is transiently induced by the photoirradiation, has been observed in cuprates [4,5], K_3C_{60} [6] and FeSe [7]. In the layered dichalcogenide 1*T*-TaS_2, stable hidden states are realized by a single femtosecond laser pulse [8].

Among them, the series of organic molecular conductor κ-(BEDT-TTF)$_2X$ (X: inorganic molecules) where BEDT-TTF is bis(ethylenedithio)tetrathiafulvalene, has a great potential for realization of photoinduced states because of their rich variety of electronic phases due to strong electron-electron interaction. [9,10] Actually, several kinds of photoinduced phenomena have been suggested near the Mott phase boundary. In the deuterated κ-Br (X = Cu[N(CN)$_2$]Br), a Mott insulator-metal transition is induced by near-infrared excitation of 0.32 eV, which is close to the inter dimer excitation of BEDT-TTF molecules [11]. Moreover, in the normal conducting state of the κ-Br, the excitation of 0.95 eV leads to a metal-Mott insulator phase separation (PIPS) [12]. Furthermore, in the recent measurements, after midinfrared excitation of 0.16 - 0.18 eV, which corresponds to the energy of vibrational mode of BEDT-TTF molecules, possible transient superconductivity has been observed significantly above the transition temperature (T_c) in κ-Br [13].

Recently, it has suggested that a visible excitation of 3.1 eV induces anomalous polarization-dependent carrier relaxation dynamics (hereafter AP dynamics) not only in κ-Br but also in κ-NCS (X = Cu(NCS)$_2$) [14], where the electronic state is located away from the Mott phase boundary. κ-NCS shows superconducting (SC) transition

[(a)] E-mail: satoshi.tsuchiya@eng.hokudai.ac.jp (corresponding author)

at T_c of ∼10 K [15]. In κ-Br, the temperature dependences of the signal amplitude and relaxation time are similar to those in κ-Cl (X = $CuN(CN)_2Cl$) [12, 16], suggesting that the Mott insulating gap emerges due to PIPS. On the other hand, in κ-NCS, the temperature dependence of the signal amplitude is different from that in κ-Br and κ-Cl [12, 16]. Moreover, the gap amplitude obtained from the theoretical fitting does not agree with that of κ-Cl. Furthermore, the origin of the polarization anisotropy is still controversial.

An optical pump broadband-probe spectroscopy is a powerful technique to reveal a wide range of photo-induced changes in the electronic spectrum. So far, this technique has uncovered the high-energy spectral change due to the SC transition and pseudogap (PG) formation in cuprates [17, 18] and κ-Br [19], as well as carrier relaxation associated with the spin-density-wave state in pnictides [20]. Therefore, by applying this technique to κ-NCS, we can obtain critical insights into the origin of the AP dynamics.

In this paper, we report the transient spectral change in the range from 1.44 eV to 1.59 eV by means of spectrally resolved optical pump-probe measurement in κ-NCS. The polarization anisotropy of the AP dynamics is found to be most enhanced at 1.51 eV, which is close to 1.41 eV of the intramolecular excitation energy of BEDT-TTF but not exactly. This difference can be reasonably thought of as the formation of an energy gap at the Fermi energy. Such gap formation leads to an increase or decrease in optical transitions from a pump induced carrier state near the Fermi energy (E_F) to a state away from the E_F by the probe energy depending on the probe polarization. Furthermore, we try to discuss the origin of the gap by comparing the size of the gap with that of possible gap states.

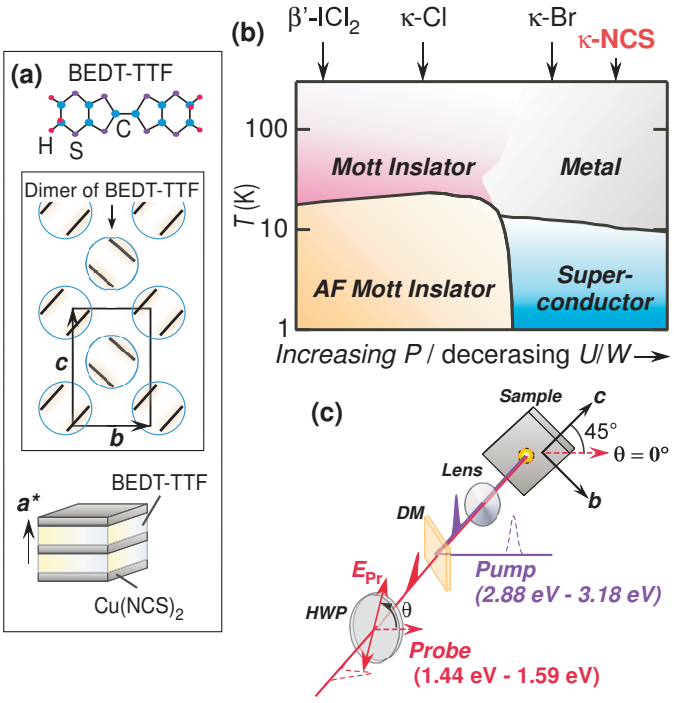

Fig. 1: (Color online) (a) (a) A schematic illustration of BEDT-TTF molecule, arrangement of BEDT-TTF molecules and crystal structure. H, S and C stand for hydrogen, sulfur, and carbon atoms, respectively. (b) The conceptual phase diagram of κ-$(BEDT\text{-}TTF)_2X$ and a related dimeric compound obtained from the recent paper [10]. AF stands for anti-ferro magnetic. (c) A schematic view of the measurement setup for polarized pump probe spectroscopy. HWP and DM stand for a half-wave plate and dichroic mirror, respectively.

Experimental. – Single crystals of κ-NCS were synthesized electrochemically [21]. Figure 1(a) shows schematic illustrations of a BEDT-TTF molecule and its arrangement. In the κ-type arrangement, the dimerized BEDT-TTF molecules are arranged in a zigzag pattern, forming a conducting layer. The conducting layers are alternately stacked with insulating layer of $Cu(NCS)_2$ along the $\boldsymbol{a}^\star$ axis. The dimensions of the crystal used in the present measurement were ∼ 700 × 600 × 50 μm^3. Figure 1(b) shows the temperature (T) vs Pressure (P) phase diagram [10]. In the κ-$(BEDT\text{-}TTF)_2X$ system, the unit cell volume changes due to the substitution of X, which can be thought of as an effective chemical pressure. In the phase diagram, an increase of P correspond to a decrease in the effective electron correlation of U/W, where U and W are the onsite Coulomb repulsion and the band width, respectively. The electronic state of κ-NCS is located farther from the Mott phase boundary than that of κ-Br.

Pump probe measurements were conducted using 120 fs laser pulses of 1.55 eV generated from a cavity-dumped Ti:sapphire oscillator with a repetition rate of 54 kHz to avoid the heating effect. To perform spectrally resolved measurement, we used pulses of $\hbar\omega_{pr}$ =1.44, 1.48, 1.49, 1.51, 1.53, 1.55 and 1.59 eV for the probe by adjusting the wavelength of the oscillator. The pump pulses ranged from 2.88 eV to 3.18 eV were prepared by the second harmonic generation of the LiB_3O_5 (LBO) crystal. According to the band structure calculation [22], the energies of probe pulses almost correspond to the next HOMO-HOMO transition, where the next HOMO and HOMO denote the next to the highest occupied molecular orbital and the highest occupied molecular orbital, respectively. The energies of pump approximate the transitions from the HOMO to bands well above the LUMO or from bands well below the HOMO to the LUMO, where the LUMO represents the lowest unoccupied molecular orbital.

Figure 1(c) shows the schematic view of the measurement setup. Pump and probe pulses were coaxially overlapped and irradiated perpendicular to the conducting plane. The pump and probe beams have diameters of ∼ 20 μm and ∼ 12 μm, respectively. To investigate the probe polarization dependence, the polarization ($\mathbf{e}_{\rm pol}$) was changed by rotation of a half wave plate (HWP). The θ is the angle of polarization measured from a direction tilted 45° form the $\boldsymbol{c}$ axis. The fluence of pump pulse was fixed

to 30 μJ/cm^2 during the measurements. For 30 μJ/cm^2, photo-excited carrier density δ is $\sim 4 \times 10^{-5}$ per dimer which is calculated under the assumption that each photon excites one carrier using the following form

$$\delta = \frac{FV_{dim}}{l_{opt}\hbar\omega}, \tag{1}$$

where $V_{dim} = 844$ Å^3 [23], $l_{opt} = 13$ μm [24] and $\hbar\omega = 3.1$ eV are the volume of a dimer, optical penetration depth and photon energy, respectively. It is assumed that the same AP dynamics can be obtained even if the pump energy is between 2.88 eV and 3.18 eV. This experiment was performed at 5 K and 50 K, where the AP dynamics was observed to be dominant, and at 100 K, where it was not.

In the pump probe measurements, the pump pulse excites carriers from the occupied states to high-energy unoccupied states. And the excited carriers relax rapidly to the electronic states above the E_F by electron-electron and electron-phonon scattering, forming non-equilibrium distribution of carriers as well as phonons [25]. The transient change of reflectivity $\Delta R/R$ observed by the probe pulses reflects the transition between the photoexcited carrier states near the E_F and the unoccupied states above the probe energy, as well as the transition between the unoccupied states near the E_F and the occupied states below the probe energy. $\Delta R/R$ is written as

$$\frac{\Delta R}{R} = \frac{R_{pump} - R_0}{R_0} \propto \Delta f N |M_{ij}|^2, \tag{2}$$

where R_{pump} and R_0 are the reflectivity with and without pump pulse irradiation and Δf, N and M_{ij} are the non-equilibrium distribution function of carriers, the density of electronic states, and the dipole matrix element, respectively. By measuring $\Delta R/R$ with delayed probe pulse, the temporal evolution of Δf can be seen. If an energy gap for electronic excitations forms, such as a SC gap or PG, a relaxation bottleneck may occur [26,27] and the dynamics undergo a great change compared to the normal state. Therefore, we can extract information on the nature of the gap at the E_F through the dynamics measurements.

Results. – Figures 2(a) shows $\Delta R/R$ as a function of θ at $T = 5$ K for $\hbar\omega_{pr} = 1.48$ eV. At $\theta = 0°$, the transient reflectivity is quite smal. As θ increases, the transient signal becomes negative at $\theta = 45°$ and then, it becomes again small at $\theta = 90°$. As θ increases further, it becomes positive $\theta = 135°$. The similar trend is observed in the other probe energies as shown in Figs. 2(b) and 2(c). Figures 2(d)-2(f) show polar plots of signal amplitude obtained from the value at 0.5 ps. At all probe energies, $\Delta R/R$ is found to enhance at $\theta = 135°$ ($\mathbf{e}_{\rm pol}//\boldsymbol{b}$). Such polarization anisotropy is consistent with that in the previous measurement, indicating that the AP dynamics are dominantly observed even when the probe energy is different.

In order to see the polarization-dependent dynamics

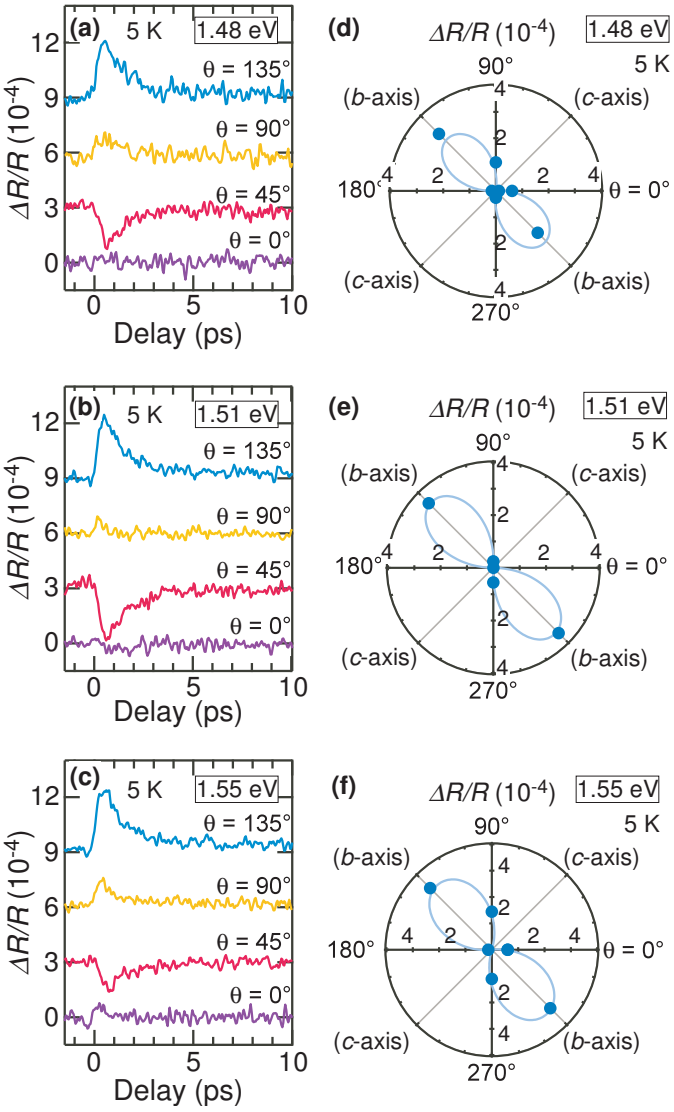

Fig. 2: (Color online) (a)-(c) Transient change of reflectivity $\Delta R/R$ for $\theta = 0°$, 45°, 90° and 135° at $T = 5$ K for $\hbar\omega_{pr} = 1.48$, 1.51 and 1.55 eV, respectively. (d)-(e) Polar plots of the amplitude of $\Delta R/R$ as a function of θ at $T = 5$ K for $\hbar\omega_{pr} = 1.48$, 1.51 and 1.55 eV, respectively. The signal amplitude is defined as the $\Delta R/R$ value at 0.5 ps. The plots show only the positive amplitude values for $\theta = 0°$, 90°, 135°, 180°, 270°, 315° and 360°. The solid lines denote the results fitted by Eq. (3).

more clearly, we decompose $\Delta R/R$ by fitting the data with the following formula,

$$\frac{\Delta R(\theta)}{R} = \frac{\Delta R_{\rm ani}}{R}\cos\left(2\left(\theta - \phi_{\rm c}\right)\right) + \frac{\Delta R_{\rm iso}}{R}, \tag{3}$$

where $\Delta R_{\rm ani}/R$ and $\Delta R_{\rm iso}/R$ are polarization-dependent (anisotropic) and -independent (isotropic) components, respectively. ϕ_c is a phase, which is a constant value of $\sim$ 130° during fitting and almost independent of the probe energy. Figures 3(a) and 3(b) show $\Delta R_{\rm ani}/R$ at $\hbar\omega_{pr} =$

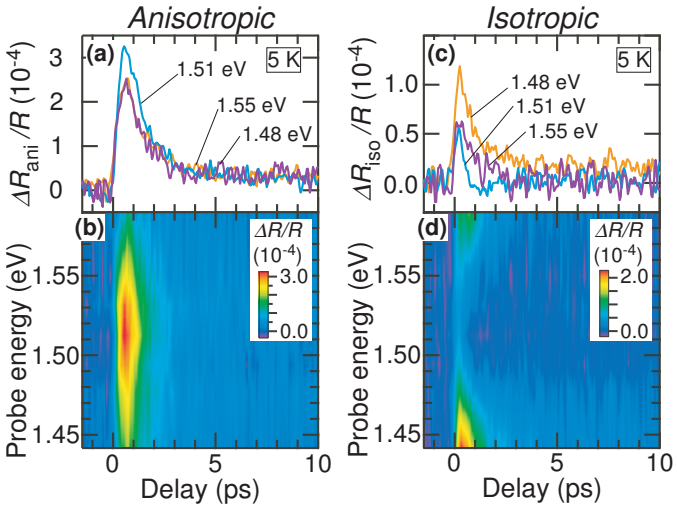

Fig. 3: (Color online) (a) $\Delta R_{\rm ani}/R$ at $T = 5$ K for $\hbar\omega_{pr} =$ 1.48, 1.51 and 1.55 eV and (b) intensity plot of $\Delta R_{\rm ani}/R$ as a function of probe energy. (c) $\Delta R_{\rm iso}/R$ at $T = 5$ K for $\hbar\omega_{pr} =$ 1.48, 1.51 and 1.55 eV and (d) intensity plot of $\Delta R_{\rm iso}/R$ as a function of probe energy.

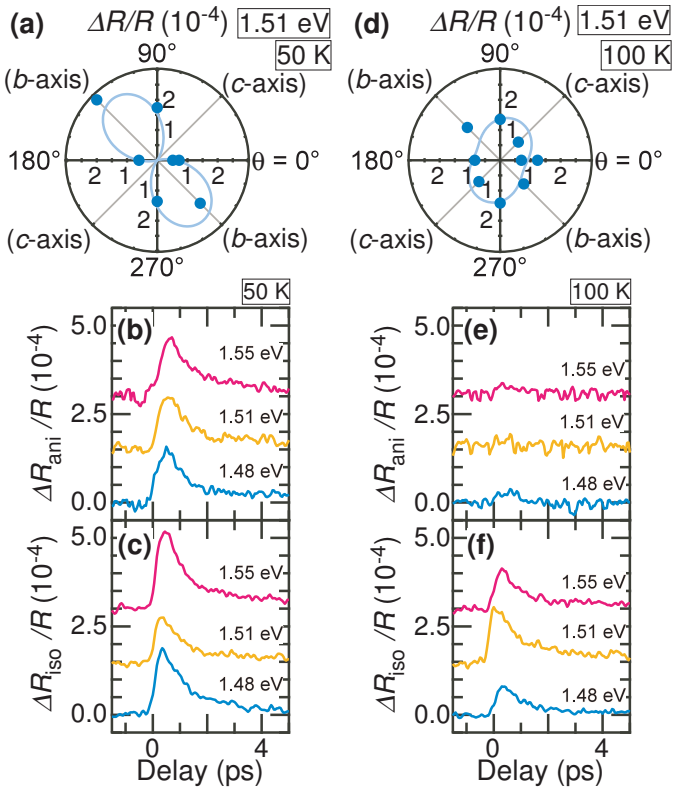

Fig. 4: (Color online) (a) Polar plots of the amplitude of $\Delta R/R$ as a function of θ for $\hbar\omega_{pr} = 1.51$ eV (a) at $T = 50$ K and (b) at $T = 100$ K. (c) Decomposed transients of $\Delta R_{\rm ani}/R$ and (d) $\Delta R_{\rm iso}/R$ at $T = 50$ K for $\hbar\omega_{pr} = 1.48$, 1.51 and 1.55 eV. (e) Decomposed transients of $\Delta R_{\rm ani}/R$ and (f) $\Delta R_{\rm iso}/R$ at $T = 100$ K for $\hbar\omega_{pr} = 1.48$, 1.51 and 1.55 eV.

1.48, 1.51 and 1.55 eV and intensity plot of $\Delta R_{\rm ani}/R$ as a function of probe photon energy. Strikingly, $\Delta R_{\rm ani}/R$ is found to be most enhanced at around 1.51 eV. On the other hand, in the isotropic component, the signal is less prominent oppositely as shown in Figs. 3(c) and 3(d).

Next, the temperature dependence of the anisotropic dynamics will be evaluated. Figures 4(a) shows polar plot of $\Delta R/R$ for $\hbar\omega_{pr} = 1.51$ eV at $T = 50$ K. The polarization anisotropy is most enhanced in the $\boldsymbol{b}$ axis direction, which is similar to that at $T = 5$ K. Figures 4(b) and 4(c) show $\Delta R_{\rm ani}/R$ and $\Delta R_{\rm iso}/R$, respectively, for $\hbar\omega_{pr}$ = 1.48 1.51 and 1.55 eV at $T = 50$ K. Both anisotropic and isotropic components seem to be dominant and somewhat dependent on the probe energy. On the other hand, at $T = 100$ K, the polarization anisotropy is less prominent as shown in Fig. 4(d). Moreover, the amplitude of the anisotropic dynamics is significantly reduced compared to the isotropic one, independent of the probe energy as shown in Figs. 4(e) and 4(f). The disappearance of the polarization anisotropy indicates that the AP dynamics is not induced at 100 K, which is consistent with the results that observed only below $T^\star \sim 70$ K [14].

To investigate the change in the anisotropic component in the spectrum, the fraction of the anisotropic component is defined as $A_{\rm ani}/(A_{\rm ani} + A_{\rm iso})$, where $A_{\rm ani}$ and $A_{\rm iso}$ are obtained from $\Delta R_{\rm ani}/R$ and $\Delta R_{\rm iso}/R$ values at 0.5 ps, respectively. Figure 5 shows the fraction as a function of the probe energy at $T = 5$ K, 50 K and 100 K. At $T = 5$ K, a peak structure is found at around 1.51 eV. As temperature increases to 50 K, the peak is kept although the fraction decreases and, at $T = 100$ K, it is not observed. Thus, the temperature-dependent results suggest that the resonance

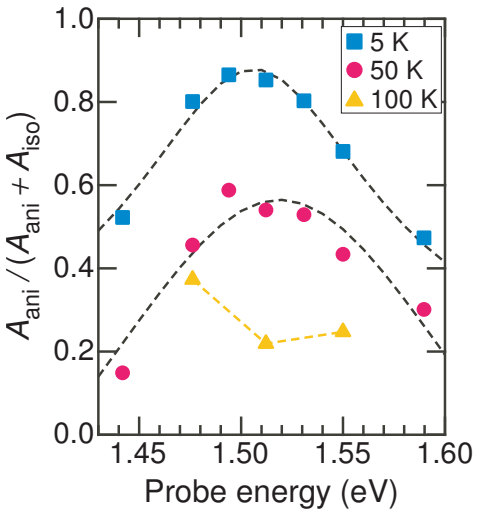

Fig. 5: (Color online) Probe energy dependence of the fraction of anisotropic component $A_{\rm ani}/(A_{\rm ani} + A_{\rm iso})$ at $T = 5$ K, 50 K and 100 K. The dashed lines are results fitted by the Lorentzian function.

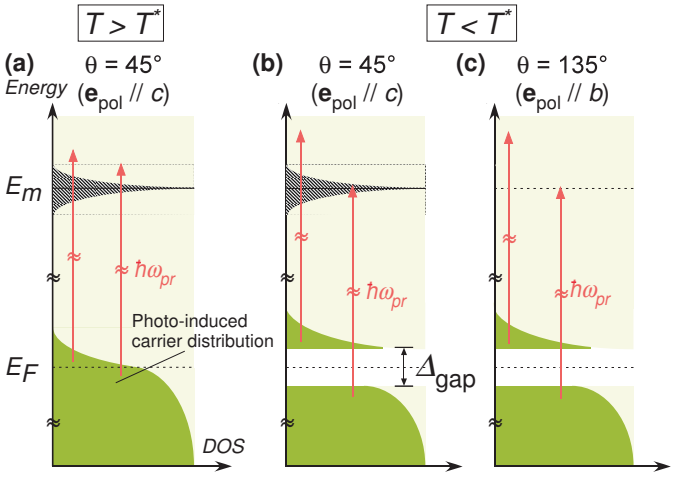

Fig. 6: (Color online) Schematic illustrations of the optical transition in the probing process (a) for $T > T^*$ at $\mathbf{e}_{\rm pol}//\boldsymbol{c}$, (b) for $T < T^*$ at $\mathbf{e}_{\rm pol}//\boldsymbol{c}$ and (c) for $T < T^*$ at $\mathbf{e}_{\rm pol}//\boldsymbol{b}$. E_m and E_F denote an intramolecular excitation energy and the Fermi energy, respectively.

at around 1.51 eV is related to the AP dynamics since the AP dynamics has only been observed below $T^\star \sim 70$ K.

We note that this criterion of the fraction is reasonable for evaluating the spectral changes in the AP dynamics in the following reason. In κ-NCS, quasi-particle dynamics originated from the SC state has been contributed to $\Delta R_{\rm ani}/R$ as well as $\Delta R_{\rm iso}/R$ below T_c. The SC dynamics is characterized by the long relaxation time of over 10 ps, whereas the AP dynamics is characterized by the fast relaxation time of ∼1 ps. Moreover, the signal amplitude of AP dynamics is about seven times larger than that of SC one at 5 K for $F = 19$ μ J/cm^2. Therefore, at 0.5 ps, the AP dynamics is more dominant than the SC one even at $T = 5$ K, which is less than T_c.

The peak energy (E_0) is estimated by the Lorentzian function,

$$L(E) = K_1 + \frac{K_2}{(E - E_0)^2 + K_3} \qquad (4)$$

where K_1, K_2 and K_3 are the fitting coefficients. The fitting goes well, yielding $E_0 = 1.51$ eV at $T = 5$ K and $E_0 = 1.52$ eV at $T = 50$ K. Moreover, a full width at half maximum (FWHM) which corresponds to a line width of resonance energy is calculated by using the K_1, K_2 and K_3 values. FWHM is obtained as 0.18 eV at 5 K and 0.14 eV at 50 K, where $K_1 = 0.1322$, $K_2 = 0.0040$, $K_3 = 0.0054$, at $T = 5$ K and $K_1 = -0.8510$, $K_2 = 0.0261$, $K_3 = 0.0184$, at $T = 50$ K.

Discussion. – Here, we discuss an origin of the resonant structure of the AP dynamics. In the pump probe measurement, the pump-excited carriers relax to the states near the E_F on the timescale of ∼100 fs. In the probing process, the transient reflectivity involves absorptions, which are given by the Fermi's golden rule. Therefore, the transitions between the photo-excited carrier state near the Fermi energy and the unoccupied state above the probe energy $\hbar\omega_{pr}$, as well as the transition between the unoccupied state near the Fermi energy and the occupied state below $\hbar\omega_{pr}$ are mainly contributed to $\Delta R/R$. Moreover, the polarization anisotropy of the probe signal $\Delta R_{\rm ani}/R$ originates from transitions that have different probabilities for each crystal axis, corresponding to the anisotropy of the matrix element of M_{ij} as indicated in the eq. (2) [28].

In the cuprate superconductor $Bi_2Sr_2CaCu_2O_{8+\delta}$ (Bi2212), two kinds of polarization-dependent carrier dynamics has been observed: one enhanced along the $\boldsymbol{a}$ axis and the other along the $\boldsymbol{a}$+$\boldsymbol{c}$ axis, which associate the SC and PG states, respectively [29]. In this case, the anisotropic change in the electronic state near E_F caused by the formation of the SC gap and PG can lead to the polarization anisotropy of the probe. However, in κ-NCS, no such gap formation was observed in the optical conductivity measurements at low energy electronic structures below $T^\star \sim 70$ K [30]. Therefore, we search for possible origins of the polarization anisotropy to the electronic states at a high energy, which is $\sim \hbar\omega_{pr}$ away from E_F.

In the optical conductivity measurements, the resonance peak is observed at $E_m = 1.41$ eV (11400 cm^{-1}) only for the direction parallel to $\boldsymbol{c}$ axis ($\mathbf{e}_{\rm pol}//\boldsymbol{c}$) at $T = 295$ K [30] which is expected to be independent of temperature. This anisotropic resonance is due to the intramolecular excitation of BEDT-TTF molecule and the E_m value is close to, but not exactly equal to, $E_0 = 1.51$ eV, which is the resonance peak position in our measurement. However, this disagreement can be considered as an indication for formation of a temperature-dependent energy gap, as discussed below. This explains why the AP dynamics appears only below $T^\star \sim 70$ K and depends on the probe polarization.

As mentioned above, in the probing process, the transient reflectivity is proportional to the photoinduced absorption. For simplicity, we consider the optical transitions from the pump-induced occupied states above and below E_F to unoccupied states away from E_F by $\hbar\omega_{pr}$ although, in principle, it is difficult to identify which optical transitions contribute to $\Delta R/R$. Figures 6(a)-6(c) show schematic illustrations in the probing process. When $T > T^*$, both transitions are not enhanced because $\hbar\omega_{pr}$ is greater than E_m as shown in Fig. 6(a). When temperature decreases below $T^\star$ and an energy gap opens at E_F, the optical transitions from the electronic states just below E_F to the states at E_m increase at $\theta = 45°$ ($\mathbf{e}_{\rm pol}//\boldsymbol{c}$), leading to an increase in the absorption as shown in Fig. 6(b). On the other hand, at $\theta = 135°$ ($\mathbf{e}_{\rm pol}//\boldsymbol{b}$), the absorption decreases because the intramolecular excited state is absent as shown in Fig. 6(c). In this way, when the energy gap is formed at E_F, the photoinduced absorption increases or decreases depending on the probe polarization and, thus, the AP dynamics appears with the resonance due to the intramolecular excitation.

From a simple calculation of $\Delta_{\rm gap}/2 = E_m - E_0$, the amplitude of the gap is roughly estimated as $\Delta_{\rm gap} = 0.20$ eV at $T = 5$ K and 0.22 eV at $T = 50$ K. In what follows, we discuss the origin of the energy gap by comparing the size of the energy gap although the gap value is only an approximation. As mentioned earlier, any type of the gap is not formed below $T^\star$ in the optical conductivity measurement, and anomalies due to some gapped state, such as a charge-ordered state, have not been reported in other measurements. Therefore, the gap is considered to be triggered by the pump pulse.

In κ-Br, the PIPS has been suggested [12, 14]. In this scenario, the 0.95 eV and 3.1 eV pump pulses can lead to modulation of electron correlation, which has a negative pressure effect on the electronic state in the phase diagram as shown in Fig. 1(b). As a result, Mott insulating state appears partially in real space, leading to microscopic or mesoscopic phase separation. κ-NCS has a similar electronic structure to that of κ-Br and a half-filled energy band, suggesting that its electronic state is discussed according to the same phase diagram of κ-Br and κ-Cl as shown in Fig. 1(b). Thus, although the electronic state of κ-NCS is further from the Mott phase boundary than that of κ-Br, similar PIPS can occur. In the Mott insulator κ-Cl, the insulating gap has been estimated as ~ 0.1 eV [31–33] and in β'-(BEDT-TTF)$_2$ICl$_2$ (β'-ICl$_2$), which has a larger U/W value than that in κ-Cl in the phase diagram shown in Fig. 1(b) [10], the effective charge gap was estimated from the transport measurements as ~ 0.28 eV at ambient pressure [34]. These values are roughly consistent with our estimation.

Another possibility is that that light irradiation can induce charge disproportionation between or within dimers of BEDT-TTF molecule. The charge disproportionation has been actively discussed in recent years not only in a quarter-filled conduction band system but a half-filled band system of κ type organic salts [35–38]. In κ-(BEDT-TTF)$_2$Hg(SCN)$_2$Cl, the conductivity spectra shows that an insulating gap due to such charge disproportionation is ~ 30 meV [36]. The value is smaller than our estimation.

Recently, the transient superconductivity has been suggested below $T = 50$ K in κ-Br [13] although the excitation energies of 0.16 - 0.18 eV were much lower than that in our measurement. In this report, photoinduced optical gap is extracted from the Mattis-Bardeen fit as a function of temperature. The zero-temperature gap amplitude was obtained to be 23 meV, which is one order of magnitude smaller than our estimation. Thus, we can conclude that the energy gap is more likely to originate from a Mott insulator than an insulator due to charge disproportionation and a superconductor.

As discussed in Bi2212 [29], when the formation of SC gap and PG is accompanied by rotational symmetry breaking of the electronic structure, the polarization anisotropy appears in the carrier relaxation dynamics. On the other hand, in general, the Mott transition is not accompanied with any symmetry breaking, indicating that photoinduced Mott gap would form isotopically. This is compatible with our scenario that the polarization anisotropy is related to the states $\hbar\omega_{pr}$ away from the electronic states near E_F.

Conclusion. – By conducting the pump probe spectroscopy with various probe pulse energy in κ-NCS, we revealed that polarization anisotropy of non-equilibrium carrier dynamics observed below $T^\star = 70$ K is attributed to the enhancement of the intradimer excitation of BEDT-TTF molecule due to the formation of an energy gap at the E_F. The gap amplitude of ~ 0.20 eV, which is obtained from the rough estimation, is consistent with that in the organic Mott insulators, indicating that the energy gap arises from the photoinduced phase-separated Mott state.

* * *

This work was partially supported by JSPS KAKENHI Grant Number 15K17685.

REFERENCES

[1] Tokura Y., *J. Phys. Soc. Jpn.*, **75** (2006) 011001.
[2] Miyano K. Tanaka T. Tomioka Y. and Y. Tokura Y., *Phys. Rev. Lett.*, **78** (1997) 4257.
[3] Chollet M. Guerin L. Uchida N. Fukaya S. Shimoda H. Ishikawa T. Matusda K. Hasegawa T. Ota A.Yamochi H. Saito G. Tazaki R. Adachi S. and Koshihara S., *Science*, **307** (2005) 86.
[4] Fausti D. Tobey R. I. Dean N. Kaiser S. Dienst A. Hoffmann M. C. Pyon S. Takayama T. Takagi, H. and Cavalleri A., *Science*, **331** (2011) 189.
[5] Hu W. Kaiser S. Nicoletti D. Hunt C. R. Gierz I., Hoffmann M. C. Tacon M. Le Loew T. Keimer B. and Cavalleri A., *Nat. Mater.*, **13** (2014) 705.
[6] Mitrano M. Cantaluppi A. Nicoletti D. Kaiser S. Perucchi A. Lupi S. Pietro P. Di Pontiroli D. Ricco M. Clark S. R. Jaksch D. and Cavalleri A., *Nature (London)*, **530** (2016) 461.
[7] Suzuki T. Someya T. Hashimoto T. Michimae S. Watanabe M. Fujisawa M. Kanai T. Ishii N. Itatani J.Kasahara S. Matsuda Y. Shibauchi T. Okazaki K. and Shin S., *Commun. Phys.*, **2** (2019) 115.
[8] Stojchevska L. Vaskivskyi I. Mertelj T. Kusar P. Svetin D. Brazovskii S. and Mihailovic D., *Science*, **344** (2014) 177.
[9] Powell B. J. and McKenzie R. H., *J. Phys.: Condens. Matter*, **18** (2006) R827.
[10] Ardavan A. Brown S. Kagoshima S. Kanoda K. Kuroki K. Mori H. Ogata M. Uji S. and Wosnitza J., *J. Phys. Soc. Jpn.*, **81** (2012) 011004.
[11] Kawakami Y. Iwai S. Fukatsu T. Miura M. Yoneyama N. Sasaki T. and Kobayashi N., *Phys. Rev. Lett.*, **103** (2009) 066403.
[12] Toda, Y. Mertelj, T. Naito, T. and Mihailovic D., *Phys. Rev. Lett.*, **107** (2011) 227002.

[13] Buzzi M. Nicoletti D. Fechner M. Tancogne-Dejean N. Sentef M. A. Georges A. Biesner T. Uykur E. Dressel M. Henderson A. Siegrist T. Schlueter J. A. Miyagawa K Kanoda K. Nam M.-S. Ardavan A. Coulthard J. Tindall J. Schlawin F. Jaksch D. and Cavalleri A., *Phys. Rev. X*, **10** (2020) 031028.
[14] Tsuchiya S. Nakagawa K. Yamada J. Taniguchi H. and Toda Y., *Phys. Rev. B*, **96** (2017) 134311.
[15] Urayama H. Yamochi H. Nozawa K. Sugano T. Kinoshita M. Sato S. Oshima K. Kawamoto A. and Tanaka J., *Chem. Lett.*, **17** (1988) 55.
[16] Tsuchiya S. Nakagawa K. Taniguchi H. and Toda Y., *J. Phys. Soc. Jpn.*, **88** (2019) 074706.
[17] Giannetti C. Cilento F. Conte S.D. Coslovich G. Ferrini G. Molegraaf H. Raichle M. Liang R. Eisaki H. Greven M. Damascelli A. van der marel D. and Parmigiani F., *Nat. Commun.*, **2** (2011) 353.
[18] Coslovich G. Giannetti C. Cilento F. Conte S.D. Abebaw T. Bossini D. Ferrini G. Eisaki H. Greven M. Damascelli A. and Parmigiani F., *Phys. Rev. Lett.*, **110** (2013) 107003.
[19] Tsuchiya S. Mertelj T. Mihailovic D. Yamada J. and Toda Y., *J. Supercond. Nov. Magn.*, **33** (2020) 2299.
[20] Pogrebna A. Vujicic N. Mertelj T. Borzda T. Cao G. Xu Z. A. Chu J.-H. Fisher I. R. and Mihailovic D., *Phys. Rev. B*, **89** (2014) 165131.
[21] Anzai H. Delrieu J. M. Takasaki S. Nakatsuji S. and Yamada J., *J. Cryst. Growth*, **154** (1995) 145.
[22] Xu Y.-N. Ching W. Jean Y. and Lou Y., *Phys. Rev. B*, **52** (1995) 12946.
[23] Oshima K. Urayama H. Yamochi H. and Saito G., *Physica C*, **153** (1988) 153.
[24] Ugawa A. Ojima G Yakushi K. and Kuroda H., *Phys. Rev. B*, **38** (1988) 5122(R).
[25] Allen P. B., *Phys. Rev. Lett.*, **59** (1987) 1460.
[26] Rothwarf A. and Taylor B. N., *Phys. Rev. Lett.*, **59** (1987) 1460.
[27] Kabanov V. V. Demsar J. Podobnik B. and Mihailovic D., *Phys. Rev. B*, **59** (1999) 1497.
[28] Dvorsek D. Kabanov V. V. Demsar J. Kazakov S. M. Karpinski J. and Mihailovic D., *Phys. Rev. B*, **59** (1999) 1497.
[29] Toda Y. Kawanokami F. Kurosawa T. Oda M. Madan I. Mertelj, T. Kabanov V. V. and Mihailovic D., *Phys. Rev. B*, **90** (2014) 094513.
[30] Sugano T. Hayashi H. Kinoshita M. Nishikida K., *Phys. Rev. B*, **39** (1989) 11387.
[31] Kornelsen K. Eldridge J. E. Wang H. H. Charlier H. A. and Williams J. M. , *Solid State Commun.*, **81** (1992) 343.
[32] Faltermeier D. Barz J. Dumm M. Dressel M. Drichko N. Petrov B. Semkin V. Vlasova R. Meziere C. and Batail P., *Phys. Rev. B*, **76** (2007) 165113.
[33] Dumm M. Faltermeier D. Drichko N. Dressel M. Meziere C. and Batail P., *Phys. Rev. B*, **79** (2009) 195106.
[34] Tajima N. Kato R. and Taniguchi H., *Europhys. Lett.*, **83** (2008) 27008.
[35] Abdel-Jawad M., Terasaki I., Sasaki T., Yoneyama N., Kobayashi N., Uesu Y., and Hotta C., *Phys. Rev. B*, **82** (2010) 125119.
[36] Drichko N., Beyer R., Rose E., Dressel M., Schlueter J. A., Turunova S. A., Zhilyaeva E. I., and Lyubovskaya R. N., *Phys. Rev. B*, **89** (2014) 075133.
[37] Mizukoshi K., Ito H., Nakamura Y., Hayama H., Yoshida Y., Saito G., and Kishida H., *J. Phys. Soc. Jpn.*, **88** (2020) 024710.
[38] Kobayashi T., Ding Q.-P., Taniguchi H., Satoh K., Kawamoto A., and Furukawa Y., *Phys. Rev. Research*, **2** (2020) 042023(R).